Title: Farmed calcite $\delta^{13}C$ at Ascunsă Cave, Romania, and its relation with CO_2 outgassing and drip rate

Virgil Drăguşin*

Emil Racoviță Institute of Speleology, Frumoasă 31, 010986 Bucharest, Romania, e-mail: virgil.dragusin@iser.ro

*corresponding author

Ionuț Cornel Mirea

Emil Racoviță Institute of Speleology, Frumoasă 31, 010986 Bucharest, Romania.

Babeș–Bolyai University, M. Kogălniceanu 1, Cluj-Napoca, Romania

Romanian Institute of Science and Technology, Virgil Fulicea 3, 400022 Cluj-Napoca, Romania

e-mail: ionut.mirea@iser.ro

Nicolae Cruceru

Emil Racoviță Institute of Speleology, Frumoasă 31, 010986 Bucharest, Romania, e-mail: cruceru nick@yahoo.com

Vasile Ersek

Department of Geography and Environmental Sciences, Northumbria University, Newcastle-upon-Tyne, NE1 8ST, UK, e-mail: vasile.ersek@northumbria.ac.uk

Laura Tîrlă

Faculty of Geography, University of Bucharest, N. Bălcescu 1, Romania, e-mail: tirla@geo.unibuc.ro

Abstract

When calcite precipitates in caves, its carbon stable isotope signature can be modified by the CO_2 outgassing gradient between drip water and cave atmosphere. This effect is modulated by water residence time in the cave, from its emergence in the cave until the deposition of calcite. Moreover, CO_2 solubility, calcite precipitation rate, and isotopic fractionation are controlled by temperature.

Here, we present up to date results of an ongoing monitoring study at Ascunsă Cave (Romania), exploring the relationship between farmed calcite $\delta^{13}C$, drip rate, and CO_2 outgassing. In addition to measuring CO_2 concentration in cave air, we also measured the CO_2 concentration in the headspace of a water-air equilibrator that collects drip water without exposing it to cave atmosphere, preventing outgassing. $\delta^{13}C$ from calcite farmed at two neighboring stalagmites with different drip rates was also measured.

Although caves have generally stable temperatures, we show here that temperature inside Ascunsă and Isverna caves has risen by more than 2°C over the course of a year, bearing important implications for stable isotopic fractionation equations and CO_2 dynamics.

Our results show that $\delta^{13}C$ of farmed calcite has a strong relationship with drip rate at the slow dripping site, but no correlation at the faster dripping site. These two sites are also different when $\delta^{13}C$ is compared to the outgassing gradient. At the slower drip site, $\delta^{13}C$ and the outgassing gradient are directly correlated, whereas at the faster drip site their correlation is inverse.

Our study brings new light onto speleothem $\delta^{13}C$ behavior in general, and at Ascunsă Cave in particular, which is crucial for understanding the paleoclimate information captured by speleothems from this cave or elsewhere.

Keywords: cave monitoring, CO_2, farmed calcite, $\delta^{13}C$, Ascunsă Cave

1. Introduction

Cave monitoring programs specifically designed for speleothem studies are meant to bring information on how speleothems are archiving environmental information. The most used environmental proxies in speleothem studies are $\delta^{18}O$ and $\delta^{13}C$, but they are influenced by a wide range of processes that act at global, regional and local scale (Fairchild and Baker, 2012; Lachniet, 2009; McDermott, 2004). At local scale, not only do these processes vary between caves, but they also vary inside the same cave, having different impacts on different speleothems.

One of the local factors that have an important imprint in speleothem $\delta^{18}O$ and $\delta^{13}C$ is the outgassing of CO_2 from the groundwater that feeds a speleothem. This process takes place both during the emergence and stagnation of a drop of water around its entry point (e.g., a stalactite tip), but also after the formation of a thin water film on top of a stalagmite (Dreybrodt, 2008).

Recently, laboratory experiments were carried out in order to test theoretical models of stable isotope dynamics (Wiedner et al., 2008; Polag et al., 2010; Hansen et al., 2019). Experimental work of Hansen et al. (2013), Hansen et al. (2017) or Dreybrodt (2019) focused on the outgassing and isotopic exchange processes taking place during the presence of a thin water film on top of a stalagmite, from which calcite precipitates. They confirmed previous theoretical studies and identified two outgassing steps. The first takes place by diffusion shortly after the formation of the thin film on the stalagmite tip. Diffusion occurs in a matter of seconds until the aqueous CO_2 equilibrates with atmospheric CO_2, irrespective of the gradient between drip water and atmosphere pCO_2, and without impacting the isotopic composition of the dissolved inorganic carbon (DIC). The second step, that does control the isotopic composition of calcite, takes place during carbonate precipitation from this chemically equilibrated solution, with a duration that is one order of magnitude longer than the first step. Moreover, Dreybrodt et al. (2016) calculated the duration of a third process related to isotopic exchange between drip water CO_2 and cave air CO_2, which is on the order of thousands of seconds.

Apart from water and air chemistry, both CO_2 outgassing and carbonate precipitation are influenced by temperature and this is one of the main parameters recorded during cave monitoring programs. This is important because caves are thought to represent stable environments, with little

temperature variability, which allows for speleothem deposition under stable conditions. Moreover, cave air temperature is thought to represent the mean surface temperature (Badino, 2004; Dominguez-Villar, 2012).

Our study presents up-to-date measurements of several parameters relevant for speleothem paleoclimatic studies at Ascunsă Cave (Romania), that were first reported by Drăguşin et al. (2017b). We aim to investigate in more detail the relationship between farmed calcite $\delta^{13}C$ on the one hand, and the CO_2 outgassing gradient between drip water and the atmosphere on the other. We also study the relationship between drip rate and farmed calcite $\delta^{13}C$, and present the variability of the calcite saturation index calculated based on pH, electrical conductivity and alkalinity of drip water.

Our results allow a better understanding of how calcite $\delta^{13}C$ responds to local factors and will help us refine its paleoenvironmental interpretation in speleothems from this cave. Speleothem stable isotope records from two stalagmites from this cave were already published by Drăguşin et al. (2014) and Staubwasser et al. (2018), but forthcoming studies will benefit from a more thorough understanding of local processes brought by the present work.

2. Materials and methods

Ascunsă Cave is located in SW Romania, at an altitude of 1050 m and is part of a larger cave system, of which Isverna Cave is the main groundwater collector and discharge point, at 450 m. In this study we used the field methods detailed in Drăguşin et al. (2017b) and focus on the monitoring point associated with the POM 2 stalagmite, in the Great Chamber, where we measured different parameters at available points, that are a few meters apart from each other (Fig. 1). For example, because the ceiling is about 10 m high, drip water for stable isotope analysis was taken from a more accessible straw stalactite population. The water-air equilibrator was installed at a different stalactite, which ensures enough recharge for the equilibrator to have constantly refreshed water and reduce CO_2 outgassing through the water column.

The water-air equilibrator is air-tight by design and there should be no gaseous CO_2 exchange with the atmosphere except through the water column (Fig. 2). The CO_2 inside the headspace, as well as other gasses in the confined atmosphere, should be at equilibrium with the accumulated water. Dripping inside the equilibrator contributes to the perturbation of the water surface, ensuring fast equilibration. Thus, any change in drip water chemistry should be reflected in the chemistry of the headspace in a relatively short time. The only way for CO_2 to escape the headspace is by being dissolved and carried away through the syphon formed at the bottom of the equilibrator and discharged into the cave. We note that we discontinued the use of a second equilibrator that was described in Drăguşin et al. (2017b), because it was behaving as a rhythmic spring and was purging all the water by syphoning.

CO_2 measurements were performed using a Vaisala GMP222 probe with an accuracy expressed as the sum of 1.5% of measurement range of the probe (in the case of our probe, calibrated for 0 to 10,000 ppmv, this a priori value translates to 150 ppmv) plus an additional 2% of the measured value. For example, for an 8000 ppmv measurement, the error would be 310 ppmv. The CO_2 values are reported at ambient temperature and pressure. Atmospheric pressure, was measured with a Sunartis BKT381 barometer. Headspace CO_2 ($CO_{2\ HS}$) is considered to be in equilibrium with dissolved CO_2, while CO_2 dissolved in water exposed to the atmosphere is considered to be in equilibrium with atmospheric CO_2. For the purpose of this study, we consider the values of $CO_{2\ HS}$ as reflecting those of dissolved CO_2 in drip water before entering the cave, while $CO_{2\ ATM}$ reflects dissolved CO_2 after equilibration with cave atmosphere values.

Air temperature and relative humidity were measured using Tinytag Plus2 data loggers. Due to condensation on the RH sensor, this parameter could not be measured reliably and will be further assumed to be close to 100%.

We installed Stalagmate drip loggers at the site of the POM 2 stalagmite described by Drăguşin et al. (2014) and at the site of stalagmite POM 10, a few meters away. The drip loggers at POM 2 and POM 10 were topped by glass plates on which water dripped and deposited calcite. We also

installed a glass plate on the nearby active stalagmite POM X. The observed drip rate at POM X is much slower than at POM 2, but similar to that at POM 10.

Stable carbon isotope ratios of farmed calcite ($\delta^{13}C$) that were not yet reported in Drăguşin et al. (2017b) were measured at Northumbria University (UK) on a Thermo Delta V Advantage IRMS coupled to a GasBench II sample preparation and introduction system. Typical measurement errors are ±0.1‰, and stable isotope values are reported on the VPDB scale.

Drip water was sampled from several drip sites, pools and water-air equilibrators in the cave and preliminary results were presented in Drăguşin et al. (2017b). In this study we focus on the samples taken from the drip site that fed the POM 2 stalagmite, and from the nearby water-air equilibrator. Water pH, as well as temperature, were measured using a WTW Sentix 41 probe, after the pH electrode was calibrated against two buffer solutions (7 and 10) that were left to equilibrate with the cave temperature. Electrical conductivity (EC) was measured using a WTW Tetra-Con 325 EC electrode. Alkalinity was determined in the field by titration using a Merck MColortest carbonate hardness test, whose semiquantitative determination could have an uncertainty as high as 30% (Vatca C., Merck, pers. comm.)

Before the installation of the drip logger at POM 2, drip water was left to accumulate in a plastic bottle from one visit to the next. After the drip logger was installed in August 2014, water could be left to accumulate in a plastic bottle only during the visit to the cave, a process that could take several hours depending on the drip rate. Due to such time constraints, in 2015 we discontinued the direct sampling of this drip point. Nevertheless, we continued to sample water from the equilibrator that is readily available and measured physical and chemical parameters until September 2017. Regarding the similarity of samples left to accumulate for long periods of time compared to those accumulated over several hours, we note that at the POM Entrance drip site, two such samples showed almost identical values for pH, alkalinity, EC and chemical composition (unpublished data). This seems to indicate that water is refreshed in the plastic bottle over the course of hours and should not be considered representative for longer periods of time.

158 Water from the equilibrator was sampled using a tube and allowed to fill the bottle by avoiding
159 turbulent flow as much as possible, in order to reduce CO_2 outgassing during the procedure.

160 Based on field measurements, we calculated the calcite saturation index following the equation
161 derived from Langelier (1936):

162 SI=pH-pHs,

163 where pH is the measured pH and pHs is the saturation pH, calculated as

164 $pHs = \{9.3 + [(\log_{10}TDS - 1) / 10] + [-13.12 \times \log_{10}(T+273) + 34.55]\} - [(\log_{10}Ca^{2+} - 0.4) +$
165 $\log_{10}ANC]$, where TDS (mg/L) =0.55 x EC (µS/cm), T(°C) is the water temperature, Ca^{2+} is
166 expressed as $CaCO_3$ (mg/L) and is calculated as ANC (mmol/L) x 50.04 mg/L.

167

168 ## 3. Results and discussion

169 **3.1. Air temperature.** The temperature logger closest to the cave entrance (POM Entrance)
170 records seasonal cycles related to the chimney effect circulation, but during 2019 a sharp 4°C rise
171 can be seen during the warm season in comparison to previous years (Fig. 3). At POM A, air
172 temperature increased by almost 2°C since January 2019 after experiencing a slight multi annual
173 increase trend of about 0.2°C. One can also distinguish subdued seasonal cycles of about 0.2°C,
174 similar in timing to those at POM Entrance, and probably linked to cave ventilation regimes. On
175 short time scales on the order of ten of hours, temperature at POM A was shown to be very stable
176 and is influenced by atmospheric thermal tides (Drăgușin et al., 2018).

177 More dramatically, at POM2 temperature rose by about 2.5°C in 2019, from ~8°C to >10.5°C,
178 where it seems to have stabilized. By comparison, the nearby Isverna Cave experienced a similar
179 2°C dramatic warming over 2016-2017, from ~10°C to ~12°C (Drăgușin et al., 2017b), followed by
180 two years when temperature remained high. Over the summer of 2019, temperature returned
181 abruptly to a value closer to 10°C.

At this point there is no clear indication to explain the rapid increase in temperature inside Ascunsă Cave during 2019. We cannot completely rule out a delay in heat transfer through bedrock, if the temperature rise in both Isverna and Ascunsă caves was produced by a warming episode of surface temperature in 2016 or earlier. Nevertheless, this is less probable, as all three points inside Ascunsă Cave start warming at the same time, even though the overburden is about 20 m at POM Entrance, 40 m at POM A and 100 m at POM 2. At Isverna Cave, the overburden is around 30 m, implying that a common surface warming would be observed roughly at the same time at Isverna and POM A (which is more stable than POM Entrance). Neither of the two caves are open to the public and are seldomly visited.

In the vadose zone of karst systems, water and air flow can alter the geothermal gradient, acting as cooling liquids (Luetscher and Jeannin, 2004; Badino, 2005; Dominguez-Villar, 2012). We can thus hypothesize that geothermalism is better expressed following the overall reduction in groundwater flux to the cave, that we measured as a general decrease in drip rate. It seems that during 2019, a threshold was crossed at Ascunsă Cave, where infiltrating water decreased so much that it lost its ability to counteract the thermal effect of rock temperature on cave air.

3.2. Drip rate at POM 2 shows a generally decreasing trend since 2014 when it stood at about 30 drips/min, punctuated by fast drip periods linked to rainfall or snow melt events (Fig. 4). The aquifer feeding the drip site reached baseline in the second half of 2017 due to lack of recharge in spring and summer, recording values of 1-2 drips/min. Higher snowmelt and spring rainfall in early 2018 recharged the aquifer, but drip rates indicate a return towards baseline in early 2019. This pattern repeated in the spring of 2019, with values decreasing later in the year. The quick response of drip rates to rainfall and snow melt indicates that the aquifer is fed via fractures, possibly mixed with seepage flow that would be responsible for maintaining baseline conditions (Baker et al., 1997).

The drip logger on the POM 10 stalagmite recorded very low values since its placement in 2016. The maximum value recorded was 1.2 drips/min in November 2019, but values did seldomly surpass 0.6 drips/min, possibly indicating a seepage flow regime. Overall, the POM 10 record

mirrors the POM 2, although at such slow drip rates even small increases appear to stand out from the generally low background.

3.3. CO_2 concentration in the headspace of the water-air equilibrator (CO_{2HS}) is several times higher than the one in the cave atmosphere (CO_{2ATM}). While the headspace values were between 6000 ppmv and 8000 ppmv, the ones in the cave atmosphere did not exceed 4000 ppmv (Fig. 5 and Table 1). $CO_{2\ HS}$ values were generally around 8000 ppmv between the summer of 2015 and the summer of 2017, but decreased to a level below 6000 ppmv by the end of 2019. Drăguşin et al. (2017b) suggested that such high values throughout the year indicate the presence of an organic matter reservoir deep inside the epikarst that continues to decompose and to produce CO_2 over the winter.

Both $CO_{2\ HS}$ and $CO_{2\ ATM}$ records show a decreasing trend over the five years of monitoring, that is steeper in the headspace values. The overall decrease in $CO_{2\ ATM}$ is very small and the trend in our data is imposed by two high values recorded at the end of 2015 and beginning of 2016. The full record sits mostly around 2000 ppmv, and it might indicate a possible modulation by other factors.

The correlation coefficient between $CO_{2\ ATM}$ and drip rate is 0.7, p-value = 0.02 (Table 2), suggesting that either CO_2 is introduced to the cave atmosphere mostly via drip water or that they might have a common process behind their covariance. At Chauvet Cave in France, Bourges et al. (2020) too, identified a link between atmospheric CO_2 and drip rates, but with an inverse correlation that was imposed by a combination of external processes that include outside air temperature and water excess. We have no estimation of CO_2 transport to the cave via open fractures as identified for example in Gibraltar by Mattey et al. (2016).

The difference between $CO_{2\ HS}$ and $CO_{2\ ATM}$, ΔCO_2, is used to describe the gradient between the CO_2 concentration in equilibrium with drip water before entering the cave, and the CO_2 concentration in water that is at equilibrium with the cave atmosphere. The correlation between CO_{2HS} and ΔCO_2 ($r = 0.8$, p-value = 0.01) indicates that ΔCO_2 is imposed by $CO_{2\ HS}$. This has relevance for the outgassing of CO_2 from drip water, as higher $CO_{2\ HS}$ values would impose a higher ΔCO_2. As we will see further, this is important for defining isotopic fractionation conditions.

Water chemistry. The pH of the POM 2 drip point ranges between 7.5 and 8.1 (Fig. 6, Table 3) and shows a negative correlation with $CO_{2\ ATM}$ (r = -0.8, p-value = 0.005). This inverse correlation could indicate that the pH of drip water reached equilibrium with $CO_{2\ ATM}$. If the pH of drip water equilibrates with cave air CO_2, it does so in a short time, on the order of seconds as suggested by laboratory experiments (Hansen et al., 2017; Dreybrodt, 2019). Moreover, the strong correlation along all the record indicates no influence of water sampling method, with no difference in behavior between plastic bottles left to accumulate drip water on the order of hours compared to those on the order of weeks. Inside the equilibrator, pH values are lower and more stable, between 7.3 and 7.7., and show no significant correlation with neither $CO_{2\ HS}$ nor $CO_{2\ ATM}$. Lower values could be explained by the higher concentration of dissolved CO_2 in drip water prior to outgassing.

Alkalinity was relatively stable at the drip site, with values between 4.7 and 5.7 mg/L H^+ (Table 3). Inside the equilibrator, values varied between 4.6 and 5.8 mg/L H^+, and the longer dataset allows one to distinguish more variability.

Electrical conductivity of the drip site was stable in the first part of the record, around ~445 μS/cm, but rose to values of ~480 μS/cm at the end of the measurement period. Water sampled from the equilibrator shows values above ~465 μS/cm for the whole period and a generally rising trend, up to ~490 μS/cm. One might also distinguish slight reductions in values during the late autumn (at the beginning and end of the record) and, more clearly, during the winters of 2015-2016 and 2016-2017.

The calcite saturation index is positive at the POM 2 drip site, with values ranging from 0.1 to 0.6. Its variability closely resembles that of pH (r = 0.9), indicating the strong control that pH has in defining the saturation index. Inside the equilibrator, the saturation index shows periods with fluctuating positive and negative values, between -0.2 and 0.3, varying in step with pH values.

If the saturation index follows cave air CO_2 evolution (mediated by the evolution of pH), it should also be influenced by the residence time of drip water at the stalactite tip and as a water film on top of the stalagmite. At high drip rates (e.g. 60 drips/min), water might not have enough time to outgas

and equilibrate with air CO_2, thus retaining a lower pH and saturation index, leading to less calcite deposition. This is obvious at POM 2, where calcite deposited on glass plates almost continuously since January 2017, when drip rate reached baseline at 1-2 drips/min, which translates to a residence time of 30-60 seconds. This might explain why there are more periods with calcite deposition at POM X, where the drip rate is similar to that recorded at POM 10, below 1 drip/min.

3.4. $\delta^{13}C$ values of farmed calcite are discussed here as being representative for the whole period the glass plates spent under the drip point. Nevertheless, we need to acknowledge that calcite deposition might not take place continuously, being ultimately controlled by the calcite saturation index of the drip water, that could itself vary during the several weeks of glass plate emplacement. Moreover, we compare isotopic values of farmed calcite to average values of CO_2 measured at the beginning and end of the deposition period, lacking a high-resolution record that could be available by using CO_2 data loggers for both $CO_{2\,ATM}$ and $CO_{2\,HS}$. We also lack data on the isotopic composition of the dissolved inorganic carbon (DIC) as a crucial parameter in calcite $\delta^{13}C$ dynamics.

POM 2 $\delta^{13}C$ shows 1‰ trend towards lower values between 2012 and 2017, from ~ -10.5‰ to ~ -11.5‰, followed by a return to almost -10.5‰ in 2019 (Fig. 7). POM X values are much more variable, with more than 2‰ amplitude.

$\delta^{13}C$ values at POM 2 and POM X are not correlated (r = -0.1). The difference between them, $\Delta^{13}C$, is important for comparisons between speleothems formed beneath relatively fast and slow drip sites, such as POM 2 on one side and POM X and POM 10 on the other side.

POM X $\delta^{13}C$ has a very good correlation with $\Delta^{13}C$ (r = 0.9, p-value = 0.0001), while POM 2 $\delta^{13}C$ and $\Delta^{13}C$ are inversely, and only moderately correlated (r = -0.5, p-value = 0.18). This strongly suggests that the difference between POM 2 and POM X stalagmites is controlled by the variability of the latter.

The correlation between drip rate and POM X $\delta^{13}C$ is inverse (r = -0.6, p-value = 0.04), with two outlier values corresponding to the periods between October 2017 to January 2018, and August

2018 to October 2018. If the two POM X outliers are omitted from the calculation, *r* becomes 0.96 (p-value = 6E-6). There is no apparent correlation between $\delta^{13}C$ and drip rate at POM 2 (Fig. 7A).

As lower drip rates translate into longer residence times of drip water, this inverse correlation can be explained by a longer precipitation time of $CaCO_3$, resulting in higher calcite $\delta^{13}C$ (Hansen et al., 2019). Longer carbonate precipitation times can also lead to calcite precipitating at the stalactite tip or upstream of the stalactite tip (prior calcite precipitation - PCP) a process that leads to higher stalagmite $\delta^{13}C$ (Fairchild et al., 2000). The occurrence of PCP would be indicated by increased ratios of minor or trace elements such as Mg or Sr to Ca (Fairchild and Treble, 2009). Although Drăgușin et al. (2017a) presented Mg/Ca values from four POM X calcite samples and several drip water samples, a forthcoming study will take a more detailed look at the chemical variability of drip water and farmed calcite at Ascunsă Cave.

$\Delta^{13}C$, the isotopic difference between the two stalagmites, is directly correlated with the average outgassing gradient, ΔCO_2 (r = 0.7, p-value = 0.03). We envisage this as being the result of a possible series of processes. Following a decrease in drip rate, the contribution of dissolved CO_2 as a source of $CO_{2\,ATM}$ also decreases, leading to an increase in ΔCO_2 if drip water dissolved CO_2 still retains high values. More importantly, slower drip rates translate to longer precipitation times of $CaCO_3$. The increase in CO_2 gradient, outgassing time, and carbonate precipitation time lead to higher $\delta^{13}C$ at POM X which further leads to higher $\Delta^{13}C$. This dynamic is particularly useful if $\delta^{13}C$ in the fast and slow drip stalagmites are compared (e.g., POM 2 versus POM 10), as larger differences in $\delta^{13}C$ between them would reflect decreasing drip rates and decreasing water availability.

One of the most intriguing results is that POM 2 $\delta^{13}C$ is inversely correlated with the average ΔCO_2 (r = -0.7, p-value = 0.01). This shows that stronger CO_2 gradients do not necessarily lead to isotopic enrichment of calcite at POM 2. Knowing that ΔCO_2 is strongly controlled by $CO_{2\,HS}$, we would expect to see a stronger link between POM 2 $\delta^{13}C$ and $CO_{2\,HS}$, but the correlation coefficient is rather weak (r= -0.4, p-value = 0.19). The correlation with $CO_{2\,ATM}$ is also weak (r = 0.4), while there is almost no correlation with drip rate (r = 0.1). Thus, it is possible that $\delta^{13}C$ at POM 2 is

315 controlled by other factors that were not taken into account in this study, such as the isotopic
316 composition of DIC. It is also possible that the effect of drip rate and CO_2 outgassing could be
317 masked or countered by other factors.

318

319 ## 4. Conclusions

320 We used drip loggers at two points with highly different drip rates and identified stalagmite POM
321 10 as being fed by a very slow drip site, <1 drip/min, while POM 2 has drip rates ranging from 1
322 drip/min at baseline to 90 drips/min after rain or snow melt events.

323 Since 2015, CO_2 concentration in the cave atmosphere was largely stable around 2000 ppmv, while
324 the concentration measured in the headspace of a stalactite-fed water-air equilibrator was as high as
325 8000 ppmv. The difference between drip water dissolved CO_2 and cave atmospheric CO_2 is
326 controlled by the former, which has constantly higher concentrations.

327 Calcite $\delta^{13}C$ at the POM X stalagmite varies within 2‰ and is strongly controlled by drip rate,
328 whereas drip rate has no impact on $\delta^{13}C$ at POM 2. Therefore, the $\delta^{13}C$ difference between
329 stalagmites from the faster dripping site of POM 2 and the slower dripping sites of POM X and
330 POM 10, could be used in the future to study past hydrological changes.

331 Analysis of drip water sampled at the drip site of stalagmite POM 2 and from inside the water-air
332 equilibrator shows that the water exposed to the cave atmosphere has a higher pH that prior to
333 entering the cave and that its pH value is in equilibrium with the CO_2 content of the cave
334 atmosphere. During the measurement period, drip water calcite saturation index, controlled by pH,
335 was always positive between 0.1 and 0.6. Since 2017 when drip rate values dropped below 10
336 drips/min calcite deposition took place more continuously at POM 2, indicating yet again the
337 control of drip rates on calcite formation and isotopic values.

338 We also observed a dramatic ~2°C rise in cave air temperature over the year 2019, that could have
339 been the result of reduced groundwater cooling of host rock and cave air. This shows that cave air
340 temperature, which controls water-calcite fractionation, is not truly stable for long periods of time

but it could be controlled by hydrology, with implications for stable isotope fractionation during calcite deposition.

Acknowledgements

This study was financially supported by the SEE/EEA 126/2019 grant (PI S. Constantin), the PN-III-P4-ID-PCCF-2016-0016 grant (PI O. Moldovan), and the SMIS 2014+ 120009 project (PI M. Vlaicu). We would like to thank two anonymous reviewers for their helpful comments.

References:

Badino G., 2004 - Cave temperatures and global climatic change. *International Journal of Speleology*, **33** (1/4), 103–113, DOI: 10.5038/1827-806x.33.1.10.

Badino G., 2005 - Underground drainage systems and geothermal flux. *Acta Carsologica*, **34** (2), 277–316, DOI:10.3986/ac.v34i2.261.

Baker A., Barnes W.L., & Smart P.L., 1997 - Variations in the discharge and organic matter content of stalagmite drip waters in Lower Cave, Bristol. *Hydrological Processes*, **11**, 1541–1555, DOI: 10.1002/(SICI)1099-1085(199709)11:11<1541::AID-HYP484>3.0.CO;2-Z.

Bourges F., Genty D., Perrier F., Lartiges B., Régnier É., François A., Leplat J., Touron S., Bousta F., Massault M., Delmotte M.,. Dumoulin J.-P, Girault F., Ramonet M., Chauveau C., & Rodrigues P., 2020 - Hydrogeological control on carbon dioxide input into the atmosphere of the Chauvet-Pont d'Arc cave. *Science of The Total Environment*, 716, 136844, DOI: 10.1016/j.scitotenv.2020.136844.

Dominguez-Villar D., 2012 – 4.5. Heat flux, in Fairchild I.J., & Baker, A. (eds.), *Speleothem Science: From Process to Past Environments*, John Wiley & Sons, Ltd, Chicester, UK, 137-147, DOI: /10.1002/9781444361094.

Drăgușin V., Staubwasser M., Hoffmann D.L., Ersek V., Onac B.P., & Veres D., 2014 - Constraining Holocene hydrological changes in the Carpathian-Balkan region using speleothem $\delta^{18}O$ and pollen-based temperature reconstructions. *Climate of the Past*, **10** (4), DOI: 10.5194/cp-10-1363-2014.

Drăgușin V., Balan S., Blamart D., Forray F.L., Marin C., Mirea I., Nagavciuc V., Perșoiu A., Tîrlă L., Tudorache A., & Vlaicu M., 2017a - Transfer of environmental signals from surface to the underground at Ascunsă Cave, Romania. *Hydrology and Earth System Sciences Discussions*, 1–23, DOI: 10.5194/hess-2016-625.

Drăgușin V., Balan S., Blamart D., Forray F.L., Marin C., Mirea I., Nagavciuc V., Oraseanu I., Perșoiu A., Tîrlă L., Tudorache A., & Vlaicu M., 2017b - Transfer of environmental signals from the surface to the underground at Ascunsa Cave, Romania. *Hydrology and Earth System Sciences*, **21** (10), 5357–5373, DOI: 10.5194/hess-21-5357-2017.

Drăgușin V., Tîrlă L., Cadicheanu N., Ersek V., & Mirea I.-C., 2018 - Caves as observatories for atmospheric thermal tides: an example from Ascunsă Cave, Romania. *International Journal of Speleology*, **47** (1), 113-117. DOI: 10.5038/1827-806X.47.1.2180.

Dreybrodt W., 2008 - Evolution of the isotopic composition of carbon and oxygen in a calcite precipitating H_2O–CO_2–$CaCO_3$ solution and the related isotopic composition of calcite in stalagmites. *Geochimica et Cosmochimica Acta*, **72** (19), 4712-4724, DOI: 10.1016/j.gca.2008.07.022.

Dreybrodt W., Hansen M., & Scholz D., 2016 - Processes affecting the stable isotope composition of calcite during precipitation on the surface of stalagmites: Laboratory experiments investigating the isotope exchange between DIC in the solution layer on top of a speleothem and the CO_2 of the cave atmosphere, *Geochimica et Cosmochimica Acta*, **174**, 247–262, DOI:10.1016/j.gca.2015.11.012.

Dreybrodt W., 2019 - Physics and chemistry of CO_2 outgassing from a solution precipitating calcite to a speleothem: implication to ^{13}C, ^{18}O, and clumped $^{13}C^{18}O$ isotope composition in DIC

and calcite. *Acta Carsologica*, **48** (1), 59–68, DOI: 10.3986/ac.v48i1.7208.

Fairchild I.J., & Baker A., 2012 - *Speleothem Science: From Process to Past Environments*. John Wiley & Sons, Ltd, Chicester, UK, DOI: /10.1002/9781444361094.

Fairchild I.J., Borsato A., Tooth A.F., Frisia S., Hawkesworth C.J., Huang Y., McDermott F., & Spiro B., **2000** - Controls on trace element (Sr-Mg) compositions of carbonate cave waters: Implications for speleothem climatic records. *Chemical Geology*, **166** (3–4), 255–269. DOI: 10.1016/S0009-2541(99)00216-8.

Fairchild I.J., & Treble P.C., 2009 - Trace elements in speleothems as recorders of environmental change. *Quaternary Science Reviews*, **28** (5–6), 449–468, DOI: 10.1016/j.quascirev.2008.11.007

Hansen M., Dreybrodt W., & Scholz D., 2013 - Chemical evolution of dissolved inorganic carbon species flowing in thin water films and its implications for (rapid) degassing of CO_2 during speleothem growth. *Geochimica et Cosmochimica Acta*, **107**, DOI: 10.1016/j.gca.2013.01.006.

Hansen M., Scholz D., Froeschmann M.L., Schöne B.R., & Spötl C., 2017 - Carbon isotope exchange between gaseous CO2 and thin solution films: Artificial cave experiments and a complete diffusion-reaction model. *Geochimica et Cosmochimica Acta*, **211**, 28–47, DOI: 10.1016/j.gca.2017.05.005

Hansen M., Scholz D., Schöne B.R., & Spötl C., 2019 - Simulating speleothem growth in the laboratory: Determination of the stable isotope fractionation ($\delta^{13}C$ and $\delta^{18}O$) between H_2O, DIC and $CaCO_3$. *Chemical Geology*, 509, 20-44, DOI: 10.1016/j.chemgeo.2018.12.012.

Lachniet M.S., 2009 - Climatic and environmental controls on speleothem oxygen-isotope values. *Quaternary Science Reviews*, **28** (5–6), 412–432, DOI: 10.1016/j.quascirev.2008.10.021.

Langelier W.F., 1936 - The analytical control of anti-corrosion water treatment. Journal of the American Water Works Association, 28, 1500–1521.

Luetscher M., & Jeannin P.Y., 2004 - Temperature distribution in karst systems: The role of air and water fluxes. *Terra Nova*, **16** (6), 344–350, DOI: 10.1111/j.1365-3121.2004.00572.x.

Mattey D.P., Atkinson T.C., Barker J.A., Fisher R., Latin J.P., Durrell R., & Ainsworth M., 2016 - Carbon dioxide, ground air and carbon cycling in Gibraltar karst. *Geochimica et Cosmochimica Acta*, **184**, 88–113, DOI: 10.1016/j.gca.2016.01.041.

McDermott F., 2004 - Palaeo-climate reconstruction from stable isotope variations in speleothems: A review. *Quaternary Science Reviews*, **23** (7–8), 901–918. DOI: 10.1016/j.quascirev.2003.06.021.

Polag D., Scholz D., Mühlinghaus C., Spötl C., Schröder-Ritzrau A., Segl M., & Mangini A., 2010 - Stable isotope fractionation in speleothems: Laboratory experiments. *Chemical Geology*, **279** (1–2), 31–39, DOI: 10.1016/j.chemgeo.2010.09.016.

Staubwasser M., Drăgușin V., Onac B.P., Assonov S., Ersek V., Hoffmann D.L., & Veres D., 2018 - Impact of climate change on the transition of Neanderthals to modern humans in Europe. *Proceedings of the National Academy of Sciences*, **115** (37), 9116-9121, DOI: 10.1073/pnas.1808647115.

Wiedner E., Scholz D., Mangini A., Polag D., Mühlinghaus C., & Segl M., 2008 - Investigation of the stable isotope fractionation in speleothems with laboratory experiments. *Quaternary International*, **187** (1), 15–24, DOI: 10.1016/j.quaint.2007.03.017.

Figures and tables

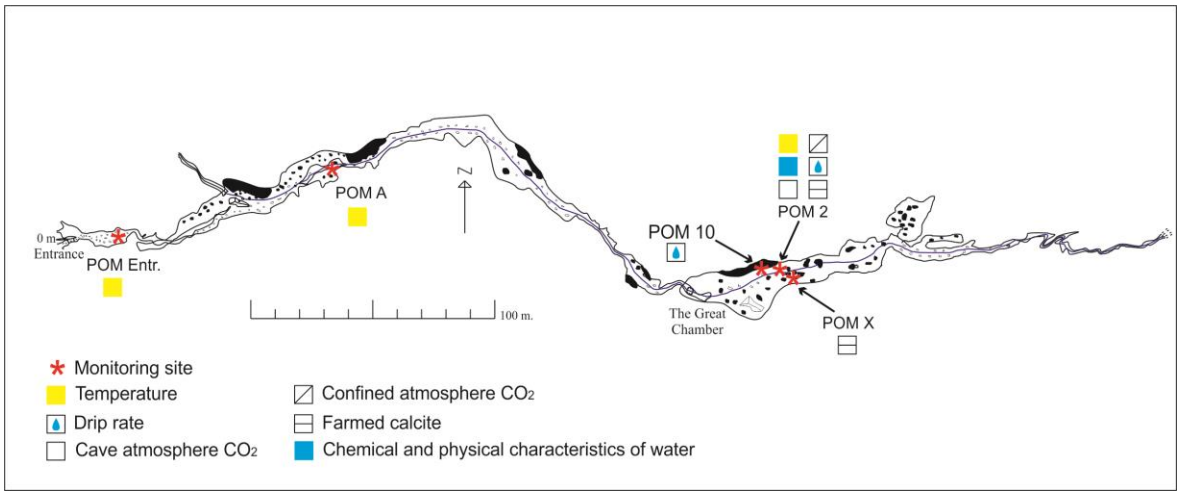

Fig. 1 – Cave map with location of monitoring points and measured parameters (modified from Drăgușin et al., 2017a).

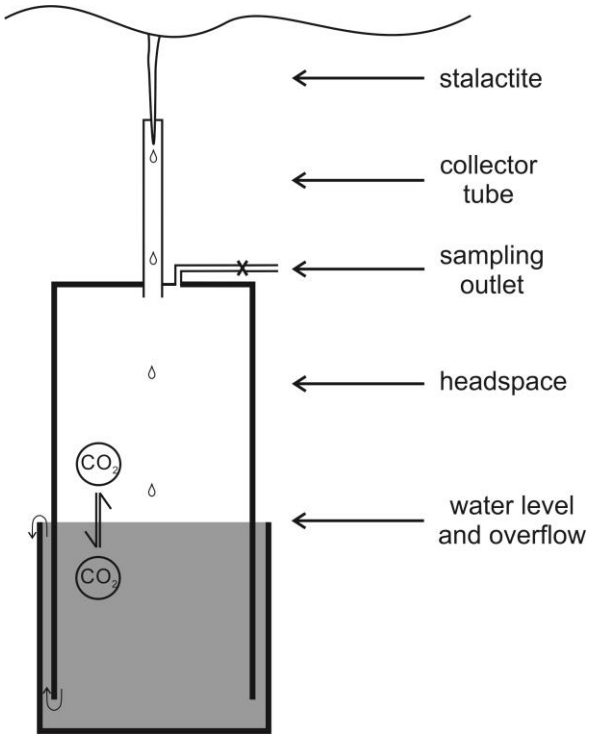

Fig. 2 – Functioning scheme of the water-air equilibrator (from Drăgușin et al., 2017a)

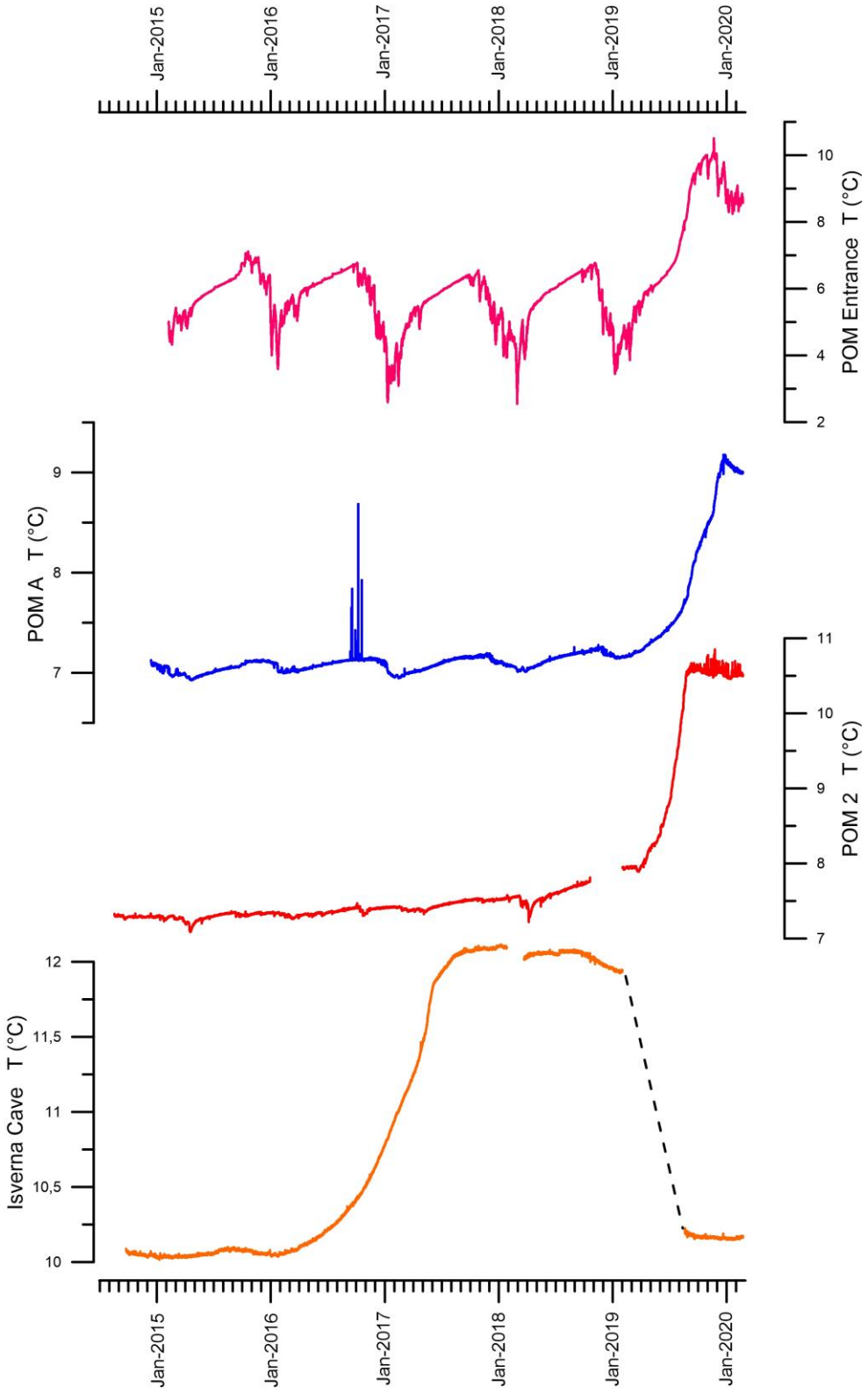

Fig. 3 – Temperature records from POM Entrance, POM A, POM 2, and Isverna Cave. During the summer of 2016, several events of higher temperature are visible at POM A, which we presume are due to the presence of bats near the logger.

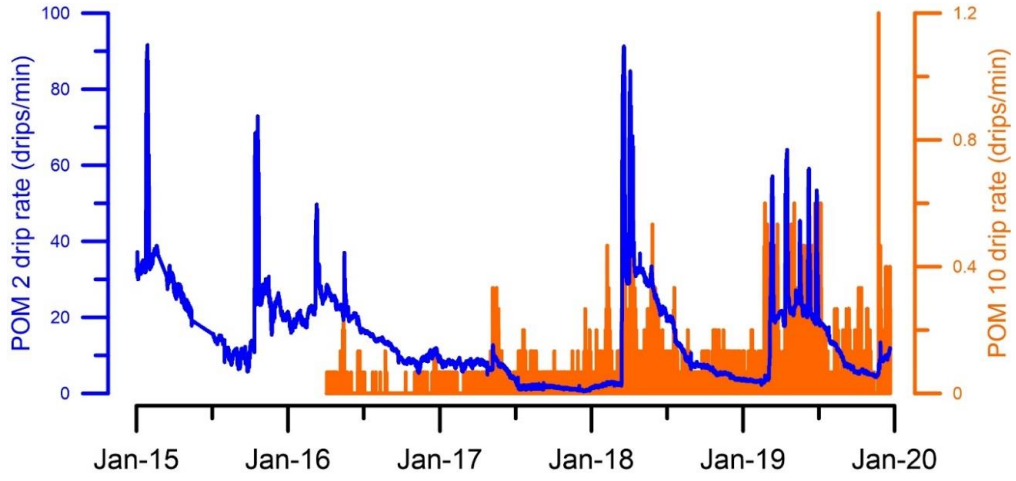

Fig. 4 – Drip rate at POM 2 and POM 10.

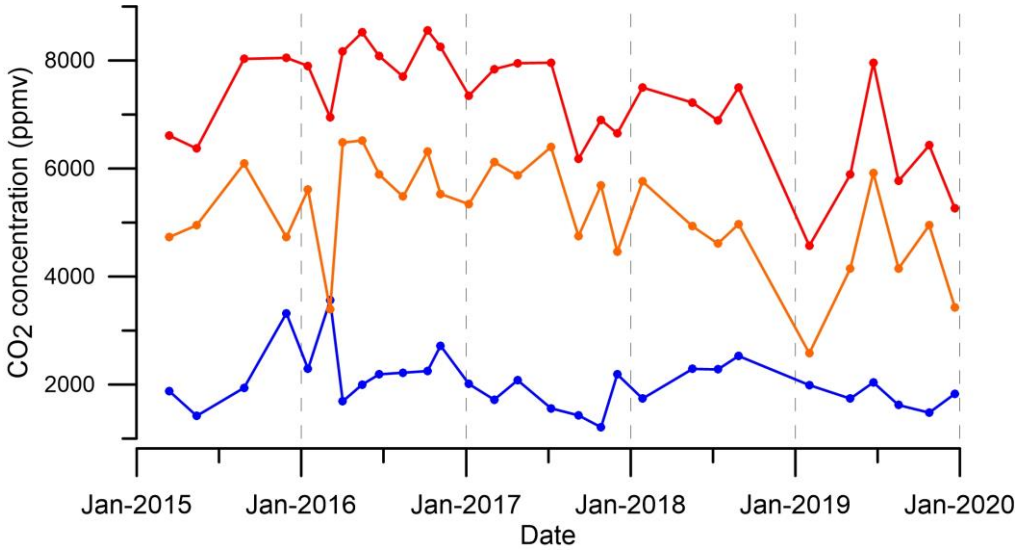

Fig. 5 – $CO_{2\,ATM}$ (blue), $CO_{2\,HS}$ (red), and $\Delta\ CO_2$ (orange).

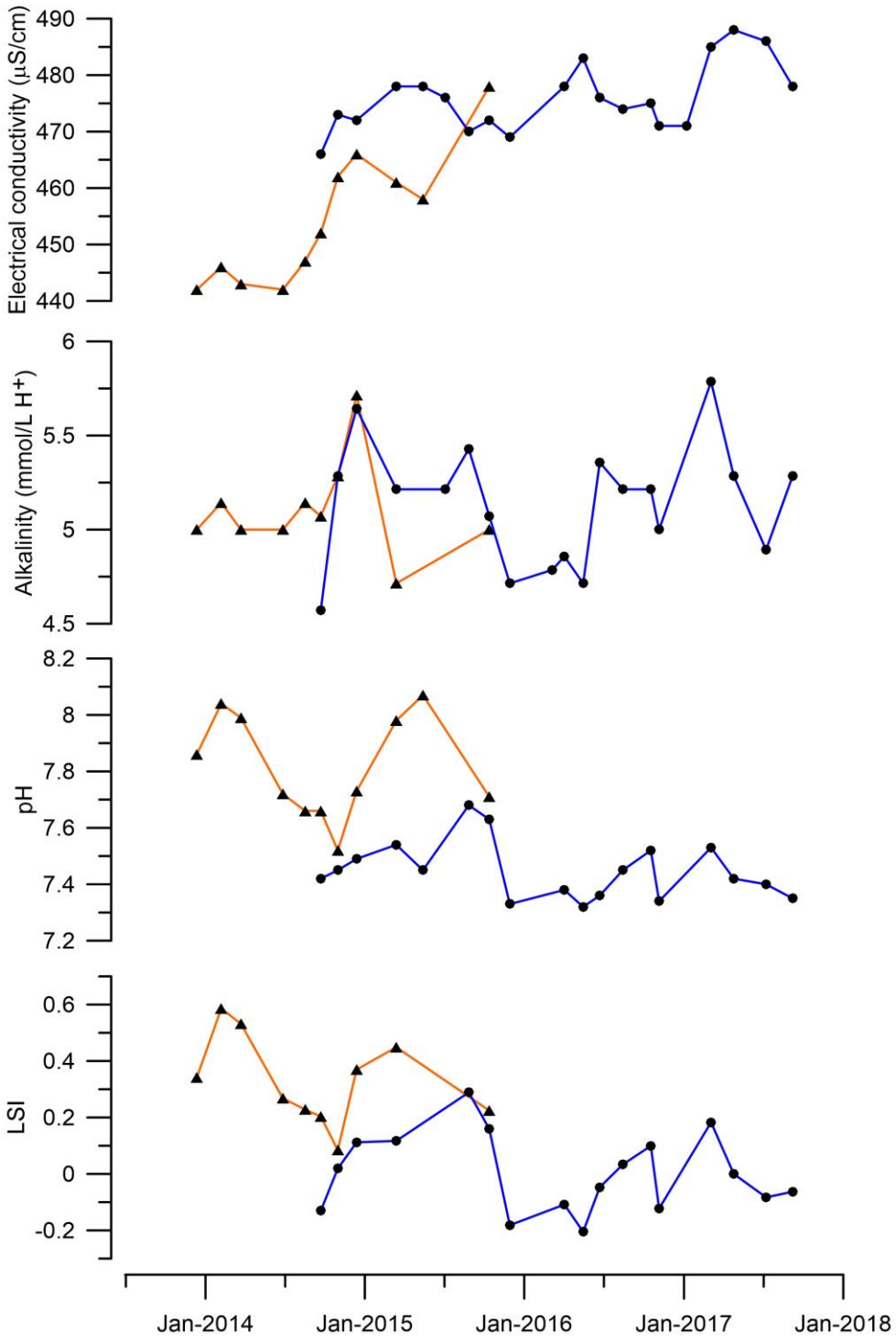

464

465 Fig. 6 – Electrical conductivity, alkalinity, pH and calcite saturation index of water samples from

466 the drip site POM 2 (triangles) and the water-air equilibrator (dots).

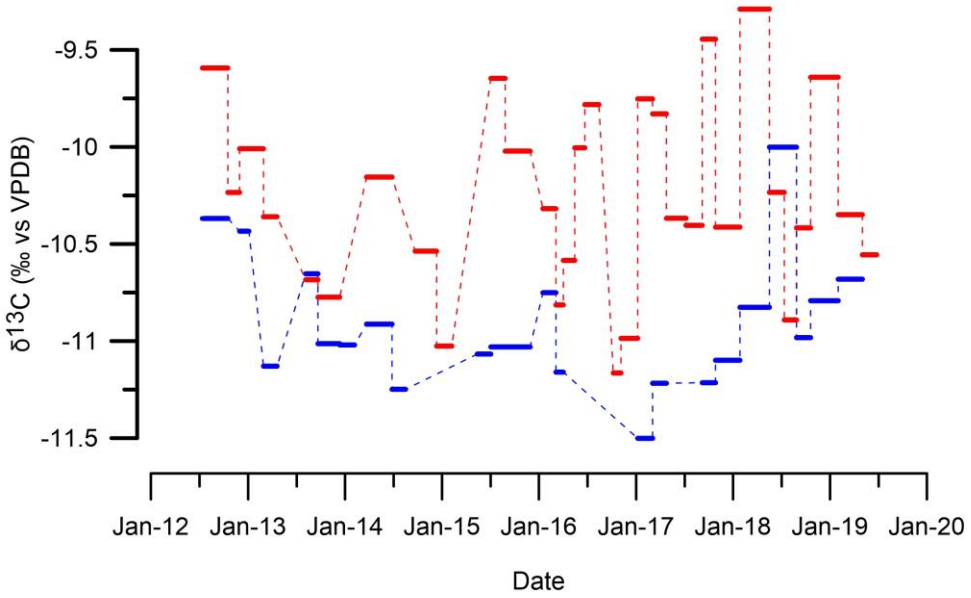

Fig. 7 - $\delta^{13}C$ of farmed calcite at POM 2 (blue) and POM X (red).

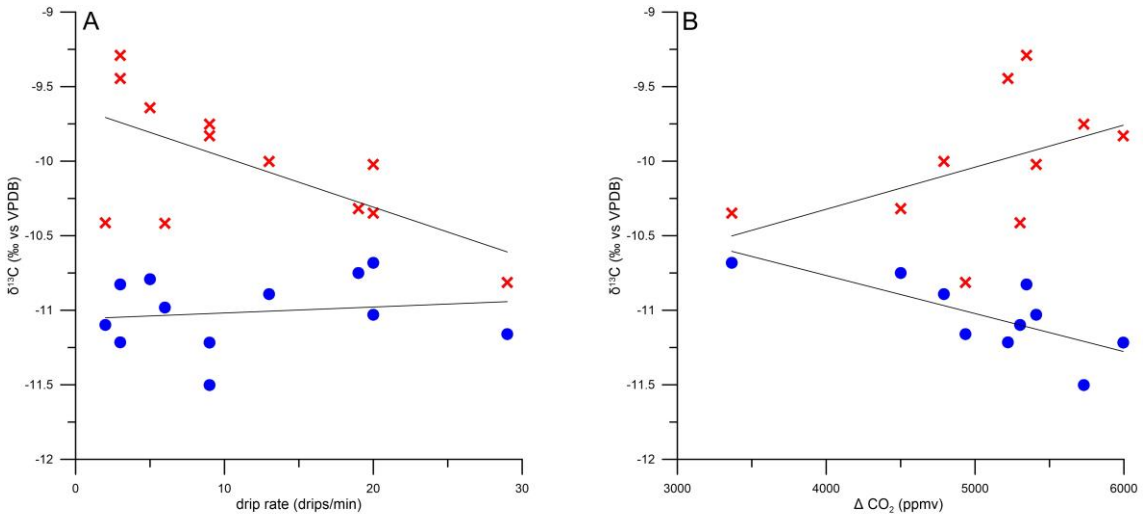

Fig. 8 – A. $\delta^{13}C$ and drip rate at POM X (red) and POM 2 (blue); B. $\delta^{13}C$ and ΔCO_2 at POM X (red) and POM 2 (blue).

Table 1. Monitoring results.

monitoring period	Average drip rate (drips/min)	POM 2 $\delta^{13}C$ (‰ vs VPDB)	POM X $\delta^{13}C$ (‰ vs VPDB)	$\Delta^{13}C$ (‰ vs VPDB)	ΔCO_2 (ppmv)	Average $CO_{2\ ATM}$ (ppmv)	Average $CO_{2\ HS}$ (ppmv)
8/15-11/15	20	-11.03	-10.02	1.01	5410	2630	8040
1/16-3/16	19	-10.75	-10.32	0.43	4500	2925	7425
3/16-4/16	29	-11.16	-10.81	0.35	4935	2625	7560
1/17-3/17	9	-11.501	-9.752	1.75	5730	1865	7595
3/17-4/17	9	-11.217	-9.830	1.39	5995	1900	7895
9/17-10/17	3	-11.215	-9.445	1.77	5220	1320	6540
10/17-1/18	2	-11.099	-10.413	0.69	5303	1713	7016
1/18-5/18	3	-10.826	-9.290	1.54	5345	2015	7360
7/18-8/18	13	-10.891	-10.001	0.89	4790	2405	7195
8/18-10/18	6	-10.982	-10.417	0.57	N/A	N/A	N/A
10/18-2/19	5	-10.792	-9.641	1.15	N/A	N/A	N/A
2/19-5/19	20	-10.681	-10.349	0.33	3365	1865	5230

Table 2. Matrix correlation between average drip rate, POM 2 $\delta^{13}C$, POM X $\delta^{13}C$, $\Delta^{13}C$, ΔCO_2, average $CO_{2\ ATM}$, and average $CO_{2\ HS}$.

	Average drip rate (drips/min)	*POM 2 $\delta^{13}C$ (‰ vs VPDB)*	*POM X $\delta^{13}C$ (‰ vs VPDB)*	*$\Delta^{13}C$ (‰ vs VPDB)*	*ΔCO_2 (ppmv)*	*Average $CO_{2\ ATM}$ (ppmv)*	*Average $CO_{2\ HS}$ (ppmv)*

Average drip rate (drips/min)	1.0						
POM 2 $\delta^{13}C$ (‰ vs VPDB)	0.1	1.0					
POM X $\delta^{13}C$ (‰ vs VPDB)	-0.6	-0.1	1.0				
$\Delta^{13}C$ (‰ vs VPDB)	-0.6	-0.5	0.9	1.0			
ΔCO_2 (ppmv)	-0.5	-0.7	0.4	0.7	1.0		
Average $CO_{2\ ATM}$ (ppmv)	0.7	0.4	-0.5	-0.6	-0.2	1.0	
Average $CO_{2\ HS}$ (ppmv)	0.0	-0.4	0.1	0.3	0.8	0.4	1.0

Table 3. Spot measurements of water samples.

Date	CO_2 ATM (ppmv)	Water T (°C)		pH		EC (µS/cm)		Alcalinity (mg/L H^+)		LSI	
		Eq.	Drip	Eq.	Drip	Eq.	Drip	Eq.	Drip	Eq.	Drip
12/12/2013	2030		5.2		7.9		442		5.0		0.3
6/2/2014	1550		7.2		8.0		446		5.1		0.6
23/3/2014	960		8.2		8.0		443		5.0		0.5
27/6/2014	1770		8.5		7.7		442		5.0		0.3
17/8/2014	2270		8.3		7.7		447		5.1		0.2
22/9/2014	2470	7.6	7.7	7.4	7.7	466	452	4.6	5.1	-0.1	0.2
31/10/2014	3440	7.3	7.0	7.5	7.5	473	462	5.3	5.3	0.0	0.1
13/12/2014	3319	7.1	7.4	7.5	7.7	472	466	5.6	5.7	0.1	0.4
14/3/2015	1880	8.3	7.2	7.5	8.0	478	461	5.2	4.7	0.1	0.4
14/5/2015	1400	7.8	6.6	7.5	8.1	478	458				
4/7/2015		8.9				476		5.2			
27/8/2015		8.1		7.7		470		5.4		0.3	
13/10/2015		7.1	7.0	7.6	7.7	472	478	5.1	5.0	0.2	0.2
29/11/2015		8.2		7.3		469		4.7		-0.2	
5/3/2016								4.8			
2/4/2016		8.1		7.4		478		4.9		-0.1	
15/5/2016		7.6		7.3		483		4.7		-0.2	
22/6/2016		7.9		7.4		476		5.4		0.0	
14/8/2016		8.6		7.5		474		5.2		0.0	
17/10/2016		8.4		7.5		475		5.2		0.1	
5/11/2016		8.1		7.3		471		5.0		-0.1	
7/1/2017		7.2				471					
4/3/2017		7.6		7.5		485		5.8		0.2	

25/4/2017		7.9		7.4		488		5.3		0.0	
8/7/2017		8.1		7.4		486		4.9		-0.1	
7/9/2017		8.2		7.4		478		5.3		-0.1	